Journal of Colloid and Interface Science 688 (2025) 140–149

Contents lists available at ScienceDirect

Journal of Colloid And Interface Science

journal homepage: www.elsevier.com/locate/jcis

Regular Article

Bridge-to-drain: How nanoparticles can promote coalescence in model polymer blends

Angela Marotta [a,1], Valentina Preziosi [a,1], Giovanna Tomaiuolo [a,b,*], Giovanni Filippone [a,**]

[a] Dipartimento di Ingegneria Chimica, dei Materiali e della Produzione Industriale, Università di Napoli Federico II, Piazzale Tecchio 80, 80125 Napoli, Italy
[b] CEINGE Biotecnologie Avanzate Franco Salvatore, Via Gaetano Salvatore 486, 80131 Napoli, Italy

HIGHLIGHTS

- Tiny amounts of nanoparticles at the interface can unexpectedly trigger coalescence.
- A novel "bridge-to-drain" coalescence mechanism has been documented.
- Particle bridging prolonged the contact time of droplets enabling matrix drainage.
- Partial surface coverage is crucial for droplet collision ending in coalescence.
- A critical droplet coverage factor was defined, above which coalescence is suppressed.

GRAPHICAL ABSTRACT

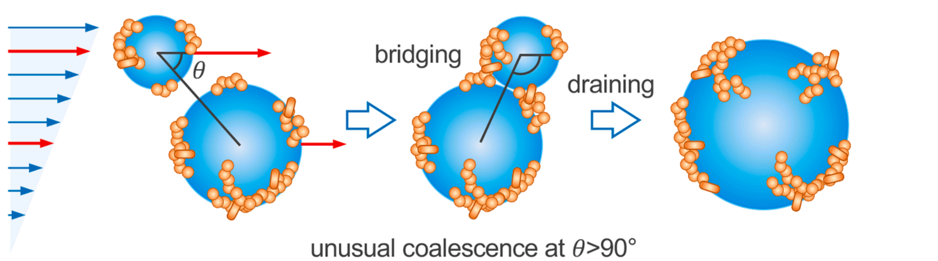

ARTICLE INFO

Keywords:
Colloids
Interface
Droplet
Emulsion
Polymer blend
Microfluidics

ABSTRACT

Hypothesis: Multiphase liquids with a droplet-in-matrix morphology are ubiquitous in many industries, from food to cosmetics and pharmaceuticals to plastics. The challenge is to control the average droplet size, which is a key parameter for the performance of the material. Nanoparticles at the droplet-matrix interface make it possible to stabilize polymer blends against coalescence. However, it has been shown that very low amounts of nanoparticles can have the opposite effect and surprisingly promote coalescence. Regardless of whether this phenomenon is desirable or not, it is important to understand it and potentially utilize it for rational design of multiphase fluids.
Experiments: We use microfluidics to unveil the mechanism of nanoparticle-induced coalescence in a model blend of polydimethylsiloxane in poly(iso)butylene (PDMS/PB 4/96 vol/vol) containing tiny amounts (up to about 0.2 wt%) of zinc oxide (ZnO) nanoparticles driven at the droplet-matrix interface via a two-step mixing protocol.
Results: Despite negligible effects on rheology and interfacial energy, the nanoparticles significantly promote coalescence. Analysis of hundreds of coalescence events revealed that the nanoparticles bridge colliding droplets and keep them in contact long enough to allow drainage of the matrix film even when the collisions occur at unfavorable angles where bare droplets do not coalesce. This novel "bridge-to-drain" mechanism requires that (i) the droplets are only partially covered by the particles and (ii) the latter have the ability to bridge droplets. A

* Corresponding author at: Dipartimento di Ingegneria Chimica, dei Materiali e della Produzione Industriale, Università di Napoli Federico II, Piazzale Tecchio 80, 80125 Napoli, Italy.
** Corresponding author.
E-mail addresses: angela.marotta@unina.it (A. Marotta), valentina.preziosi@unina.it (V. Preziosi), g.tomaiuolo@unina.it (G. Tomaiuolo), gfilippo@unina.it (G. Filippone).
[1] Equal contributions.

https://doi.org/10.1016/j.jcis.2025.02.122
Received 21 November 2024; Received in revised form 14 February 2025; Accepted 17 February 2025
Available online 18 February 2025

dimensionless critical surface coverage fraction was defined, above which the nanoparticles stop promoting coalescence and start stabilizing the microstructure.

1. Introduction

Coalescence is the main responsible for the increase in average droplet size in emulsions and blends with droplets larger than ~1 μm, where other coarsening mechanisms such as Ostwald ripening can be neglected. Coalescence is usually undesirable in the food, cosmetic and pharmaceutical industries, where the goal is to maintain finely dispersed hydrophobic (resp. hydrophilic) substances in an aqueous (or oily) continuous (i.e. matrix) phase over a long period of time [1–4]. Similarly, suppression of coalescence is a goal in the plastics industry, where immiscibility is the norm due to the negligible mixing entropy of polymers, and the challenge is to keep the dispersed phase (the droplets) as small as possible to maximize the mechanical properties [5–8]. However, coalescence is sometimes desirable to demulsify liquid mixtures, which is the case, for example, in oil recovery, wastewater treatment and sludge removal [9,10]. Regardless of whether coalescence is desirable or not, being able to control it is of paramount importance in the myriads of areas where immiscible liquids are involved.

Coalescence begins with the collision of a pair of droplets and ends with the drainage and eventual breakup of the thin matrix film between the droplets. The success of a collision, i.e. its ability to eventually lead to coalescence, depends on "external" and "internal" factors such as duration, frequency and energy of collisions, interfacial energy, bulk and interfacial rheology of both phases [11]. All these parameters can be influenced, some more, some less, by the addition of fine particles that accumulate at the droplet-matrix interface [12]. The most common effect is coalescence suppression. In general, one of the phases wets the particles more than the other, with the more poorly wetting liquid becoming the dispersed phase [13]. Since the energy required to remove a solid particle from a liquid–liquid interface is generally much higher than k_BT, interfacial adsorption can be considered irreversible and the particles remain trapped at the droplet-matrix interface, forming a layer that prevents coalescence [14]. Other stabilization mechanisms have been also invoked, such as the entrapping of the droplets in a three-dimensional network of particles that forms in the continuous phase, the reduced interface mobility due to an increased interfacial elasticity, or the occurrence of droplet clustering phenomena due to particle bridging [15–24]. Much rarer are the cases in which the opposite effect is observed, namely coarsening due to the (nano)particles. The underlying microscopic mechanism of this phenomenon is still unclear. When the particles are preferentially wetted by the droplet phase, a bridging-dewetting mechanism originally proposed to explain the anti-foaming effect of hydrophobic particles [25–29] can be invoked to explain coarsening in emulsions and blends [30,31]. However, particles that are

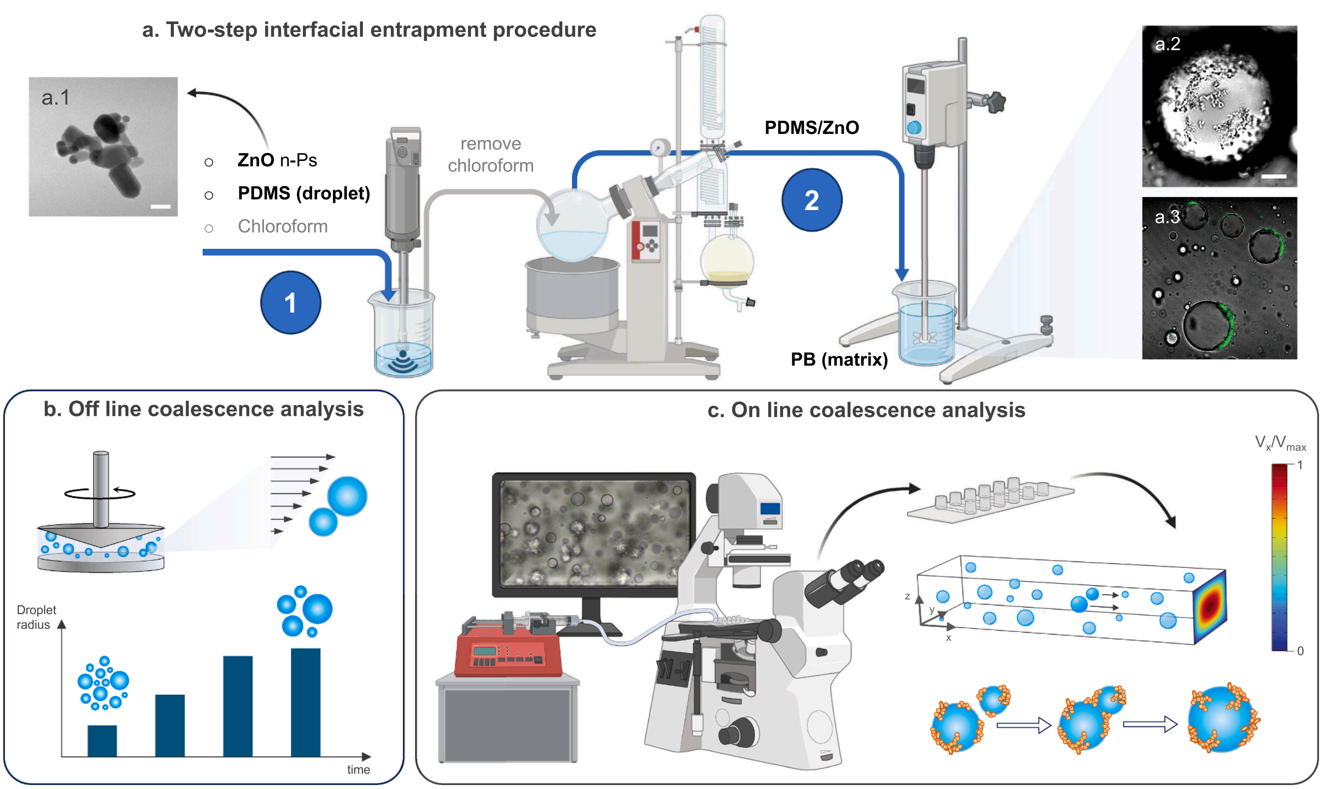

Fig. 1. Concept and workflow of the bridge-to-drain coalescence analysis. **a.** Schematic of the experimental procedure for the entrapment of the ZnO nanoparticles at the interface between PDMS (droplet phase) and PB (matrix phase). Step 1: dispersion of the nanoparticles (TEM image in a.1, scale bar 50 nm), suspended in chloroform, in the less affine PDMS phase. An ultrasonic homogenizer was used, and the chloroform was removed through a rotatory evaporator. Step 2: addition of PDMS (with or without ZnO; dispersed phase) to PB (continuous phase) and mixing with a mechanical stirrer. Bright field (a.2, scale bar 50 μm) and confocal (a.3, scale bar 50 μm) images show the localization of ZnO nanoparticles at the PDMS/PB (droplet-matrix) interface in the sample containing 0.12 (a.2) and 0.04 wt% (a.3) of ZnO. **b.** Schematic representation of the offline coalescence analysis, consisting in the measurement by image analysis of droplet radius after shearing at constant shear rate ($\dot{\gamma} = 1\ s^{-1}$) for different time in a plate-cone rotational rheometer. **c.** Sketch of the experimental apparatus used for the on-line analysis of coalescence mechanism, consisting in the exploitation of a microfluidic chip placed onto the stage of an inverted microscope, and connected to a syringe pump to impose the flow rate. The microchip contains rectangular microchannels that impose a pseudo-paraboloidal velocity profile to the flowing model blend. The live monitoring of the coalescence events elucidates the role played by the ZnO nanoparticles in promoting coalescence. Created in https://BioRender.com.

preferentially wetted by the matrix phase are known to stabilize emulsions/blends [22,23,32]. Unusual observations that contradict this picture have puzzled many researchers. In this context, it is worth mentioning the work of Velankar and co-workers, who observed particle-induced coalescence in polymer blends characterized by very small amounts of filler, regardless of which phase preferentially wets the particles [31,33–35]. The authors conjectured a key role of partial surface coverage and assumed that coalescence involves such particle-free portions of the droplets, but the lack of real-time analysis of the coalescence events prevented elucidation of the exact mechanism. Similar hypotheses were also put forward later [36,37], but to date the exact mechanism underlying particle-induced coalescence is still unclear.

Here, we unveil the origin of this phenomenon through the systematic study on a model blend of polydimethylsiloxane (PDMS) in poly(iso) butene (PB) (PDMS/PB 4/96 v/v) filled with very low amounts (max 0.21 wt%) of ZnO nanoparticles trapped onto the surface of the PDMS droplets by means of a specific two-step mixing protocol (Fig. 1a). Coalescence was studied both off- and on-line, analyzing hundreds of coalescence events by exploiting microfluidics (Fig. 1b). The latter is particularly well suited to reveal the fundamental mechanisms of morphology evolution in multiphase systems [38], also under non-dilute conditions, which are relevant for many practical applications. The composition of the selected system is similar, for example, to the typical compositions found in the mechanical recycling of plastics, when the imperfect sorting process and the presence of additives and impurities result in blends with highly unbalanced composition containing traces of fine particles. We prove that, in similar cases, substantial morphology coarsening can be induced because of a coalescence mechanism that we named "bridge-to-drain", which requires (i) a *bridging* capacity of the particles, which prolongs the duration of the contact between colliding droplets beyond what dictated by the external flow, and (ii) the presence of nanoparticle-free regions on the surface of the droplets to allow for the *drainage* of the matrix film. Above a critical droplet coverage factor, in fact, the bridge-to-drain mechanism is no longer possible, and the nanoparticles suppress coalescence as in ordinary Pickering emulsions or (nano)particle-stabilized blends [39].

2. Materials and methods

2.1. Materials

The liquid phases are polydimethylsiloxane (PDMS, Silicone oil M 10,000 by Carl Roth; nominal viscosity: 10,000 cSt, density: 0.98 g/cm^3) and poly(iso)butene (PB, Indopol H-50 by INEOS Oligomers; nominal viscosity at 100 °C 100 cSt, density: 0.95 g/cm^3). These two grades were chosen to deal with a blend having viscosity ratio at room temperature p =1. Zinc oxide (ZnO) nanoparticles (Sigma-Aldrich; nominal particle size: <100 nm, specific surface area ranging from 10 to 25 m^2/g) were used as filler. TEM analyses reveal the anisotropic shape of these nanoparticles, which comprise hexagonal, spherical, and tubular particles. The chloroform used as solvent to disperse the nanoparticles into the oils was purchased by Sigma Aldrich and used as received.

2.2. Blend preparation

PDMS-in-PB blends with and without ZnO nanoparticles were prepared following a two-step procedure. First, homogeneous suspensions of nanoparticles in PDMS were obtained by adding 2 mL of a ZnO suspension in chloroform to 20 mL of PDMS. The suspension was obtained by sonicating for 2 h (2s ON/1s OFF) at 40 % power using an ultrasonic probe sonicator (FS-450 N, Ultrasonics). The concentration of the suspensions was varied from 0.1 to 0.5 g/mL to obtain PDMS containing a mass fraction $\phi = 1, 3$ and 5 wt% ZnO. The chloroform was removed by using a rotatory evaporator. Second, unfilled or ZnO-filled PDMS was added to PB ((PDMS-ZnO)/PB 4/96 v/v) and mixed with an IKA mechanical stirrer equipped with a 20 mm diameter impeller with helical geometry. The mixing was conducted for all samples at 300 rpm for 10 min. The maximum overall content of ZnO nanoparticles was ~0.21 wt %.

2.3. Nanoparticle characterization

The surface energy of the ZnO nanoparticles (γ_{ZnO}) was evaluated by performing contact angle measurements using water, diiodomethane, and formamide. Droplets of the testing liquids were deposited onto ZnO tablets obtained by pressing the powder using a pellet press die (compacting pressure ~500 MPa). The contact angles were measured by using the LB-ADSA plug-in of the ImageJ software [40].

The localization of the nanoparticles at the interface was assessed by confocal observation via a confocal laser scanning microscope (LSM 510 META, Zeiss) equipped with a helium/neon laser (LASOS LGK 7786P) taking advantage of the autofluorescence property of ZnO particles.

2.4. Rheological analysis

Steady state shear tests were performed to measure the viscosity of the samples (η) using a stress-controlled rotational rheometer (mod. AR-G2 by TA Instruments) equipped with a Peltier plate. Measurements were carried out in cone-plate configuration (cone diameter 40 mm, cone angle 0.349 rad) at 25 °C. Steady state flow tests were conducted by varying the torque in the range 5–5000 μN·m. Frequency sweep tests were also performed to measure the elastic (G'), viscous (G''), and complex viscosity (η^*) of the samples by setting a strain amplitude of 10 % strain and varying the angular frequency from $\omega = 500$ to 0.1 rad/s.

2.5. Coalescence measurements

Off-line coalescence events were observed after shearing the sample at different strain units (s.u. $= \dot{\gamma} \times t$) at a fixed shear rate $\dot{\gamma} = 1$ s^{-1}. The latter was chosen low enough to ensure that the Capillary number (Ca ≅0.084) is well below the critical value for drop breakup (Ca_{crit} ≅0.4, as predicted by the Grace curve [41]). A strain controlled rotational rheometer (mod. ARES L.S. by Research scientific) in cone-plate configuration (diameter 25 mm, cone angle 0.0401 rad) was used for this purpose (see Fig. 1b). After shearing, small amounts of sample were carefully collected with a spatula placed under an optical microscope (mod. BX53MRF by Olympus) equipped with an LC30 digital camera for observations. Image analysis was employed with an open access software (ImageJ) to analyze the droplet size. About 500 droplets were measured per each sample, and the number-(R_N) and volume-average droplet radius (R_V) were estimated as $R_N = \frac{\sum N_i R_i}{\sum N_i}$ and $R_V = \frac{\sum N_i R_i^4}{\sum N_i R_i^3}$, where R_i is the droplet radius and N_i the number of droplets with radius R_i.

In situ coalescence dynamics were studied through a microfluidic device sketched in Fig. 1c. It consists in a polycarbonate microchannels (microfluidic ChipShop) with rectangular section (0.7 × 1.25 mm^2) placed on the stage of an inverted optical microscope (Zeiss Axiovert 100) equipped with a high-speed video camera (Phantom 4.3). A syringe pump (Harvard 11 plus) was used to impose the flow rate of the samples in the microchannels to 0.08 ml hr^{-1} (Reynolds number $Re \cong 5 \times 10^{-6}$).

A Zeiss Plan-Neofluar 63x/1.25 immersion objective was used, and videos of coalescence events were collected and subsequently analyzed with the Image-Pro Plus 6.0 software. Interfacial energy measurements were also performed by measuring the shape relaxation time of sheared droplets after cessation of the flow in a cylindrical microcapillary (diameter 320 μm, length 5 cm) following a procedure described in detail elsewhere [42].

Statistical analysis was performed using the opensource JASP software (JASP Team 2024).

3. Results

3.1. Interfacial localization and bridging capacity

The localization of (nano)particles in binary mixtures of immiscible liquids is the result of a complex interplay between thermodynamics and kinetic factors [39]. The wetting coefficient of the particles (w) predicts their localization at thermodynamic equilibrium, but metastable configurations can establish depending on the blending procedure and the rheology of the phases [43,44]. In the case under consideration, wettability calculations indicate that the ZnO nanoparticles exhibit a slight preference for the PB matrix phase (w_{ZnO} ≅1.3). This is also confirmed by their higher long-term stability in that phase compared to PDMS (Supplementary material, S1). To achieve interfacial localization, a two-step procedure was adopted (Fig. 1a): first, the nanoparticles, suspended in chloroform with the aid of an ultrasonic probe, were pre-dispersed in the less affine PDMS phase; second, after removing the chloroform, the PDMS/ZnO suspension was mixed with the preferred PB phase. This procedure successfully trapped the nanoparticles at the droplet-matrix interface, where aggregates of primary particles can be recognized. Interfacial localization was also confirmed by confocal focus stacking (Fig. 2 and Supplementary material, V1), which excludes the presence of nanoparticles inside the PDMS droplets, i.e. within the phase in which they were initially pre-dispersed.

Note that alternative mixing protocols, e.g. pre-dispersing the ZnO in the preferred PB phase or simultaneously mixing the nanoparticles and the polymers, lead to the localization of the nanoparticles in the PB matrix (Supplementary material, S2), in agreement with their higher

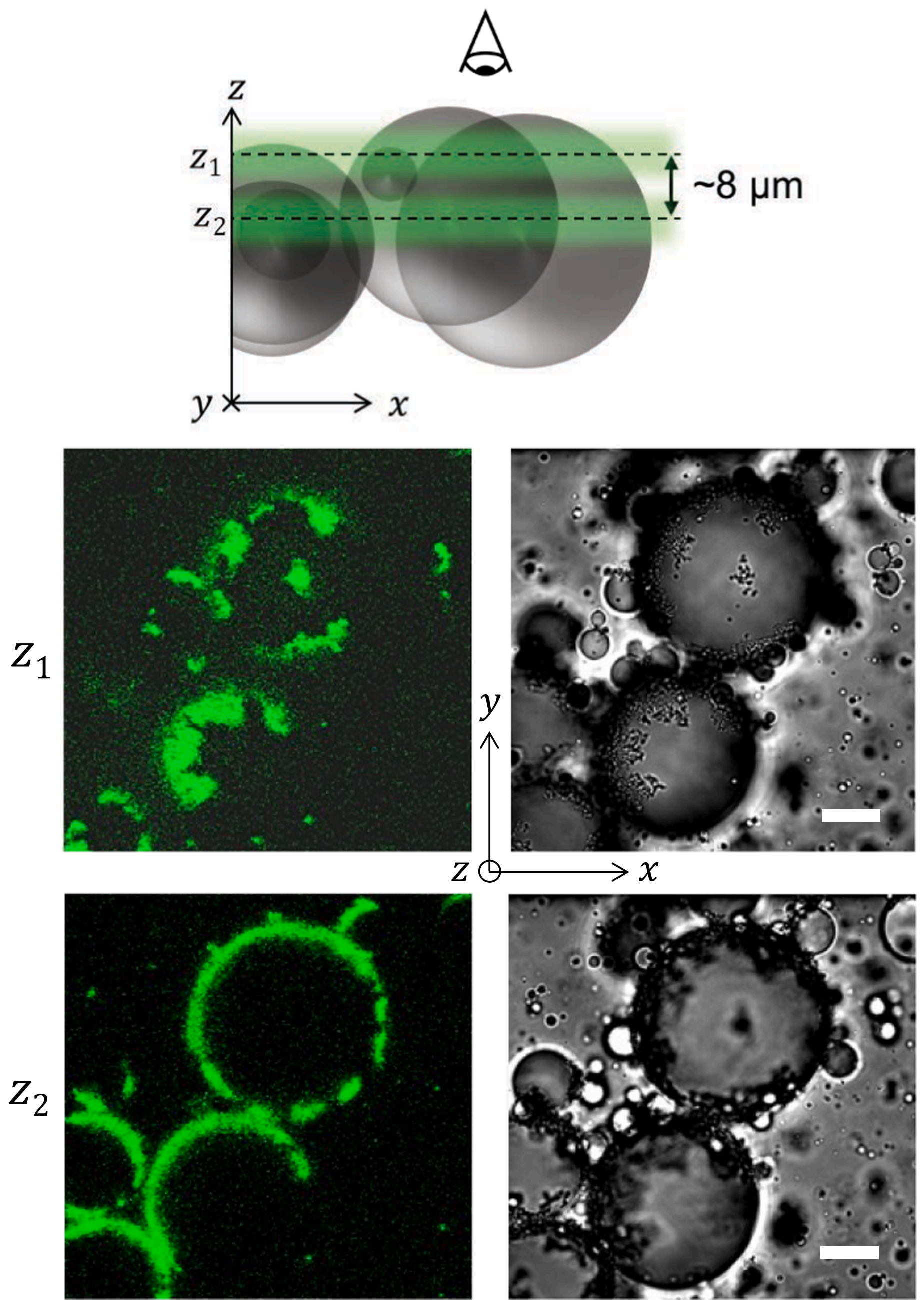

Fig. 2. Confocal (left) and bright field (right) z-stacking of the as-prepared sample at 0.21 wt% of ZnO showing the patchy coverage of the PDMS droplets (z_1) and the ability of the ZnO nanoparticle to bridge the droplets (z_2). The distance between the planes $z = z_1$ and $z = z_2$ is 8 μm. The scale bar is 10 μm. The full z-stack video is shown as Supplementary material, V1.

thermodynamic affinity with that phase. It is important to observe that the nanoparticles do not saturate the PDMS droplet surface, even at the highest loading considered in this study (~0.21 wt%). Moreover, clusters of PDMS droplets held together by bridges of particles/particle aggregates were occasionally noticed, especially at high ZnO content. The bridging mechanism, which could involve either a shared particle monolayer or multiple layers joined through particle–particle interactions, is known to occur in case of (nano)particles with higher affinity towards the matrix phase trapped at the droplet-matrix interface, which is the case under consideration. Since bridged droplets hardly coalesce, bridging is considered as one of the possible stabilizing mechanisms that preserve fine microstructures in emulsions and blends [22,37,45–47]. Another interesting aspect emerged during image acquisition regards the dynamics of quiescent coalescence events sporadically noticed especially in samples at low nanoparticle loadings. Such events always involved nanoparticle-free portions of the droplets. Moreover, droplet merging implied a quick rearrangement of the ZnO nanoparticles, which, however, remained well adsorbed on the surface of the final droplet. This can be appreciated in Fig. 3, showing two frames just before (3.a) and soon after (3.b) the coalescence of two droplets partially covered with nanoparticles in the sample at 0.04 wt% of ZnO (the full video is provided as Supplementary material, V2).

The stability of the interfacial localization reflects the high trapping energy of sub-microparticles at liquid–liquid interface [48,49] which is of order of $\sim 10^3$ $k_B T$ for $\sim 10^2$ nm sized nanoparticles. A direct consequence of interfacial trapping is that, since the overall polymer–polymer interface decreases in size after each coalescence event, the particles lie on an increasingly smaller interface, which may eventually become saturated.

3.2. Nanoparticle-induced coalescence

Because of the very low amounts of nanoparticles considered in the present study, neither the rheological properties (viscosity and linear viscoelasticity) nor the interfacial energy significantly changed after addition of the filler (see Supplementary material, S3 and S4). Nonetheless, the nanoparticles had a remarkable effect on the coalescence process promoted by slowly shearing the samples at $\dot{\gamma} = 1$ s^{-1}. The growth of R_N is shown in Fig. 4 as a function of the strain units for samples at different ZnO content (numerical data available in the Supplementary material, S5). All samples coarsen during time, the average droplet radius R_N approaching a limiting value ($R_{N\infty}$) after ~18,000 s.u. (corresponding to shearing for ~5 h at $\dot{\gamma} = 1$ s^{-1}). However, the growth is much faster and of greater magnitude in the presence of nanoparticles. Moreover, the effect is not monotonic, reaching a maximum in the sample with 0.12 wt% of ZnO.

The ability of the nanoparticles to promote coalescence is not unprecedented, having been already noticed in polymer blends and low viscosity emulsions [34–37]. What our system has in common with those in which the phenomenon was previously observed is the very low particle content, which means partial interfacial coverage. This seems to be a key requisite for the observed phenomenon to be appreciated. The ability of the nanoparticles to promote coalescence indeed reaches a maximum in the sample containing 0.12 wt% of ZnO, apparently decreasing above this threshold. To elucidate the mechanism(s) underlying this ability, as well as to explain its saturation at a certain filler content, the coalescence process has been investigated in detail by means of rheo-optical analyses.

3.3. Theoretical background and rheo-optical analyses

Droplet collision is the premise for coalescence, whose frequency, ψ, is the product of a collision frequency, C, and a collision efficacy, λ, $\psi = C\lambda$ [50]. The former parameter is dictated by external flow ($\dot{\gamma}$) and droplet size, scaling as $C \sim \frac{\dot{\gamma}}{R^3}$ in case of monodisperse droplets with radius R in shear flow [51]. Since the external flow and the initial average droplet radius are essentially the same for all systems, the initial conditions are the same and the origin of the promoted coalescence in the presence of nanoparticles must be sought in the effect of the nanoparticles on λ. The latter is defined as $\lambda = \exp(-\tau_d/\tau_c)$, where τ_d is the time needed to drain out the matrix film (thickness h) between the colliding droplets, and τ_c is the duration of the contact [50,52]. Following Chesters [11], the drainage time can be estimated by modelling the thinning of the matrix film during the contact ($-dh/dt$) and setting τ_d as the time needed for $h(t)$ to reach a critical thickness for film rupture, h_c. The solution depends on the mobility of the droplet-matrix interface, which sets the boundary conditions of the flow of the matrix film squeezed between the droplets. In our case, in which matrix and droplets exhibit comparable viscosity, the most reasonable assumption is that the droplet-matrix interface is "partially mobile". This assumption leads to the following scaling law reported in Eq. (1) for the drainage time τ_d [11]:

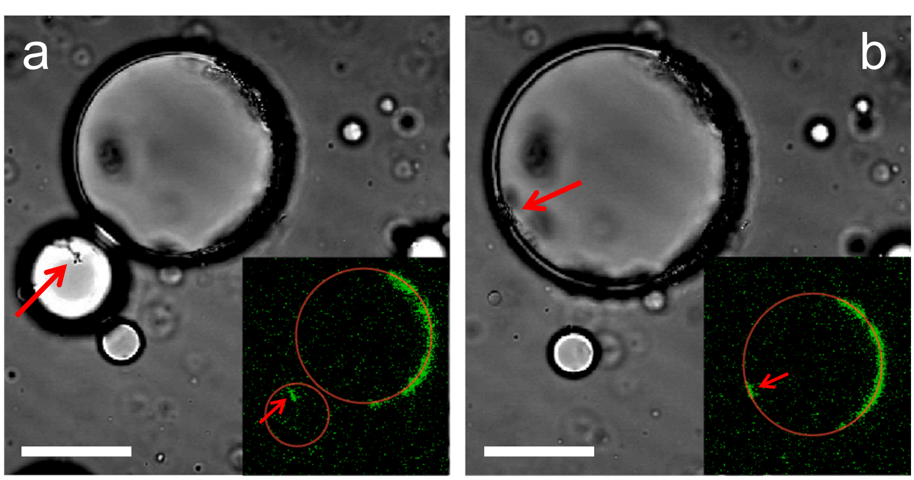

Fig. 3. a. and **b.** Confocal micrographs showing a pair of PDMS droplets just before (a) and soon after (b) a coalescence event in the sample containing 0.04 wt% of ZnO. The time interval between the two pictures is 1 s. The scale bars are 20 μm. The arrows highlight a ZnO aggregate initially lying on the surface of the smaller droplet (a) and finally reallocated on the surface of the final droplet (b). The insets show the same pictures in which only the ZnO nanoparticles are highlighted (green channel). The full video is provided as Supplementary material, V2. (For interpretation of the references to colour in this figure legend, the reader is referred to the web version of this article.)

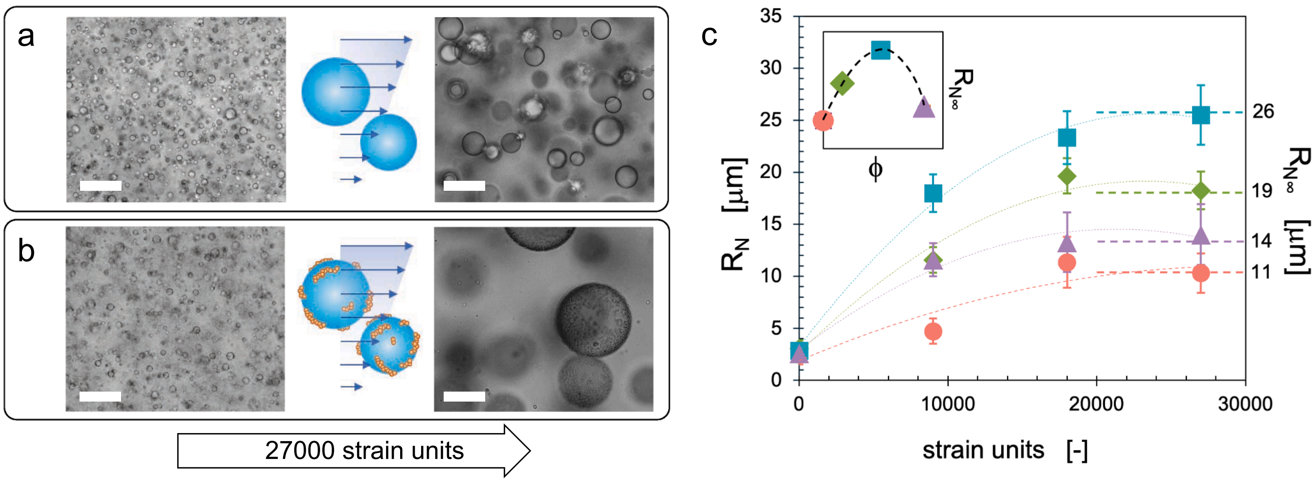

Fig. 4. **A** and **b.** Representative optical micrographs showing the evolution of the PDMS droplet size after shearing for 27,000 strain units (a: unfilled blend; b: blend with 0.12 wt% of ZnO). Bars are 25 µm. **c.** Evolution of the number average droplet radius as a function of the strain units for unfilled (orange circles) and ZnO-filled blends at different nanoparticle content: 0.04 (green diamonds), 0.12 (turquoise squares), and 0.21 wt% (lilac triangles). Lines are guides for the eye. The error bars are the standard errors. Sample size: n = 1875 (without ZnO nanoparticles), 1124 (0.04 wt% of ZnO), 869 (0.12 wt%), and 1357 (0.21 wt%) observations in different points of the sample; three independent samples analyzed per each composition. The inset shows the non-monotonic dependence of the limiting droplet radius (R_{N_∞}) on particle content. (For interpretation of the references to colour in this figure legend, the reader is referred to the web version of this article.)

$$\tau_d \propto \left[\frac{\pi\eta_d F^{1/2}}{2(2\pi\gamma/R)^{3/2}}\right]\frac{1}{h_c} \tag{1}$$

where η_d is the viscosity of the droplet phase, R is the radius of the droplets, and F is the collision force between the droplets. An expression for h_c was derived by assuming that the matrix film pierces when Van der Waals attractions become of comparable magnitude with the forces due to the radial pressure gradient in the film [11]:

$$h_c \sim \left(\frac{AR}{8\pi\gamma}\right)^{1/3} \tag{2}$$

In Eq. (2), A is the Hamaker constant and γ is the interfacial energy. Regarding F, the hydrodynamic force that acts along the line of centers of droplets colliding in shear flows squeezing the matrix film is [51]:

$$F \sim \eta_m \dot{\gamma} R^2 \sin[2(\pi/2-\theta)] \tag{3}$$

in which η_m is the viscosity of the matrix phase and θ is the angle formed by the trajectory of the droplets and the line connecting their centers.

Substituting Eqs. (2) and (3) into (1), and considering that η_m, η_d, and γ are weakly dependent on the presence of the nanoparticles, the following scaling relationship is obtained, in which only the dependence on the parameters relevant to our purpose have been made explicit:

$$\tau_d \propto \frac{\dot{\gamma}^{1/2} R^{13/6} (\sin[2(\pi/2-\theta)])^{1/2}}{A^{1/3}} = \frac{\xi}{A^{1/3}} \tag{4}$$

In Eq. (4), the numerator $\xi = \dot{\gamma}^{1/2} R^{13/6} (\sin[2(\pi/2-\theta)])^{1/2}$ reflects the collision conditions (i.e. the impact angle, local shear rate, and droplet radius), while the presence of the nanoparticles is hidden in the value of the Hamaker constant. The latter is a measure of the attractive Van der Waals force between two bodies interacting across a medium: if the collision involves bare droplets or nanoparticle-free portions of droplets, the Hamaker constant is that of pure PDMS interacting across PB; if the collision involves nanoparticle-laden portions of the droplets, one can assume that the interaction is that between ZnO nanoparticles across PB. Note that the very low dielectric constant of the selected polymers (relative dielectric constant ε_r ~2.25 for PB and ~2.85 for PDMS) makes negligible the contribution of repulsive screened electrostatic forces between the ZnO nanoparticles, which can be reasonably assumed to interact only through van der Waals forces [54,55].

To test the effect of nanoparticles on the drainage time, hundreds of coalescence events were analyzed with the rheo-optical apparatus of Fig. 1c. The coalescence process was monitored by recording the time evolution of the wall-to-wall distance between pairs of droplets, h, during approach until contact, and then measuring the duration of the drainage of the matrix film until merging, τ_d (Fig. 5).

Since, in general, coalescence involved droplets with different radius (R_1 and R_2), and relative velocity ($\Delta v = |v_1 - v_2|$), an equivalent radius,

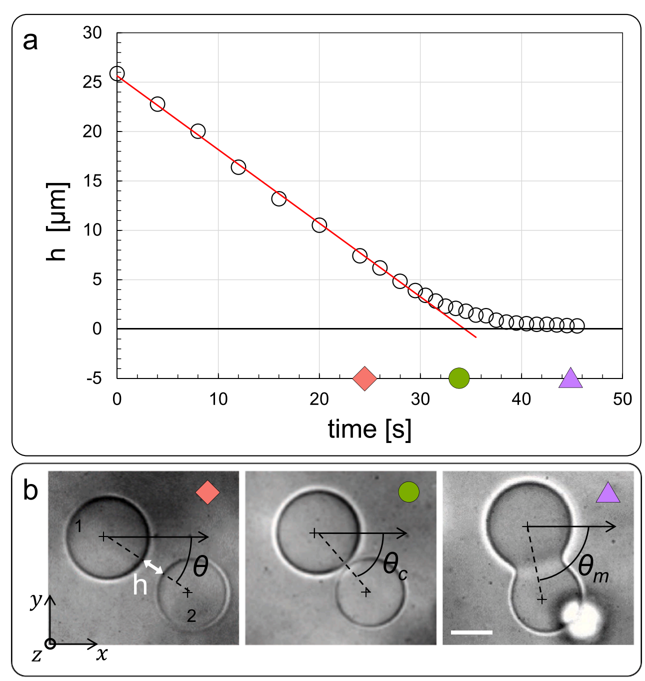

Fig. 5. Analysis of a coalescence event. **a.** wall-to-wall distance between pairs of droplets as a function of time during a coalescence event: The droplets, moving at relative velocity $\Delta v = |v_1 - v_2|$, came into contact when h approaches 0, and eventually merge when the matrix film between the droplets has been drained out (drainage time τ_d). The angle θ increases during approaching, reaching θ_c at contact and θ_m at merging. **b.** Images of the approaching droplets at different time. Scale bar is equal to 5 µm.

$R_{eq} = 2\left(\frac{R_1 R_2}{R_1+R_2}\right)$, and a local shear rate, $\dot{\gamma}_l \sim \frac{\Delta v}{R_{eq}}$, were used in place of R and $\dot{\gamma}$, respectively. Note that, since the matrix film thickness is much smaller than the radii of the droplets, the use of R_{eq} is reasonable and widely accepted in case of micrometric droplets [11]. Moreover, a geometrical correction was performed to account for coalescence between droplets moving on different focal planes (see Supplementary material, S6). This enabled us to analyze a high number of coalescence events to draw robust, statistically relevant conclusions.

The observed enhanced coalescence could derive from a reduction in the drainage time due to stronger van der Waals interactions in the presence of the ZnO nanoparticles. The τ_d values are reported in Fig. 6a as a function of ξ. For all the systems, the data lie on a straight line as predicted by Eq. (4), with slope $\tau_d/\xi \sim A^{-1/3}$.

Considering that the Hamaker constant of ZnO nanoparticles interacting across PB is ∼4 times larger than that of bare PDMS droplets (Supplementary material, S7), one should expect a lower slope of the lines in Fig. 6a for the filled samples. Instead, the slopes do not seem to change appreciably. This is shown in Fig. 6b, where the values of τ_d/ξ for the various samples at different ZnO content are compared. The non-parametric Kruskal-Wallis test indicates that data are not statistically different.

The fact that the drainage dynamics are not affected by the particles reflects the low energy required to displace them from the droplet–droplet contact area [56]. Thus, when two partially covered droplets collide, the particles move laterally away from the contact point, and leave a particle-free region in which coalescence proceeds with unchanged dynamics. The mechanism is illustrated in Fig. 6c, where the main steps of a coalescence process between two vertically contacted droplets (i.e. along the z-axis, see Fig. 6c1) are shown for the sample with 0.12 wt% ZnO. The full video is provided as Supplementary material (V3). After particle drift and formation of the circular nanoparticle-free region (6.c2), the drainage process continues until the matrix film becomes thin enough to pierce (6.c3). Then the neck connecting the droplets grows (6.c4), dragging the nanoparticles with it, which then re-accumulate on the surface of the final droplet (6.c5). Similar dynamics were observed during coalescence of partially covered oil-in-water Pickering droplets [57]. In that case, however, coalescence was halted before completing because of particle interfacial crowding, resulting in highly non-spherical doublets. Here, the particle surface coverage is too low to arrest the coalescence process, which, hence, proceeds with the same kinetics as in unfilled blends.

Since τ_d is not appreciably altered by the nanoparticles, some other mechanism must be responsible for the dramatic increase in coalescence efficiency shown in Fig. 4. Going back to the concept of collision efficacy, and having excluded the effect of the drainage time, we focus on τ_c, i.e. the time the droplets stay in contact. In unfilled blend it is usually set as the reciprocal of the local shear rate experienced by the droplets, $\tau_c = \dot{\gamma}_l^{-1}$ [11]. Here, what emerged by analyzing the coalescence events is that things change in the presence of the nanoparticles on the surface of the droplets. In particular, when two of such partially covered droplets came into contact, their dynamics appear to be no longer independent: they stick together and start moving as a single doublet. This coupling is due to the bridging ability of the considered nanoparticles (see Fig. 2), whose preference for the PB matrix make them to protrude outside the host droplet, possibly "hooking" a second droplet during collisions. This prolongs the contact time, so that even collisions at unfavorable angles become effective in the presence of nanoparticles and lead to coalescence. This picture is corroborated by the observation of several unusual coalescence events in the samples with high nanoparticle content (0.12 and 0.21 wt%). In particular, we found pairs of droplets that coalesced after the fastest droplet had already overtaken

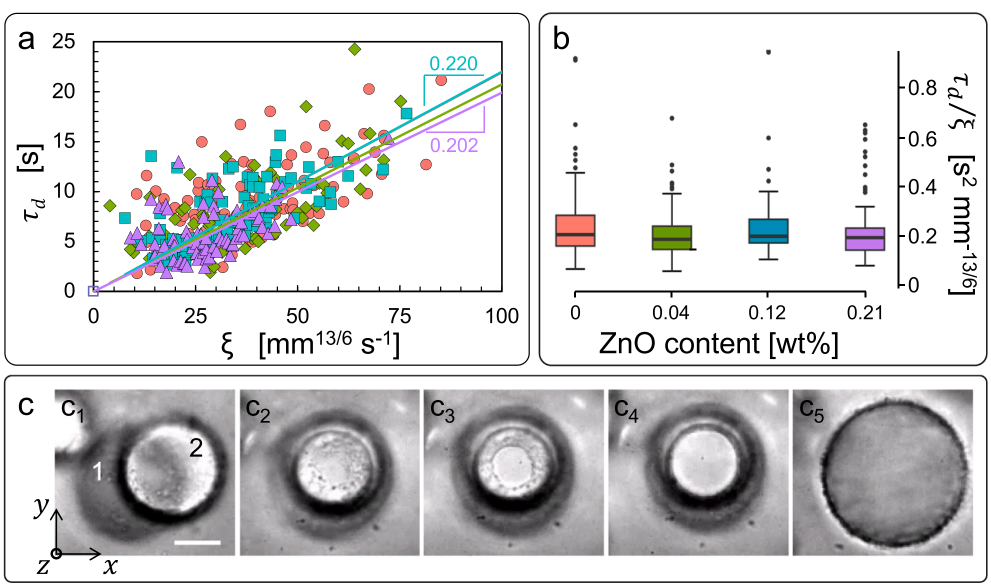

Fig. 6. **A.** Drainage times as a function of ξ for the unfilled (orange circles) and ZnO-filled blends at different nanoparticle content: 0.04 (green diamonds), 0.12 (turquoise squares), and 0.21 wt% (lilac triangles). Sample size: n=106 (without ZnO nanoparticles), 92 (0.04 wt% of ZnO), 85 (0.12 wt%), and 81 (0.21 wt%). Lines are the linear fittings to the experimental point according to Equation (4). The slopes are: 0.219 s^2 $mm^{-13/6}$ (unfilled blend, orange line, $R^2 = 0.89$, standard error (SE) = 0.008); 0.207 s^2 $mm^{-13/6}$ (sample at 0.04 wt%, green line, $R^2 = 0.88$, SE = 0.008); 0.220 s^2 $mm^{-13/6}$ (sample at 0.12 wt%, turquoise line, $R^2 = 0.91$, SE = 0.008); 0.202 s^2 $mm^{-13/6}$ (sample at 0.21 wt%, lilac line, $R^2 = 0.85$, SE = 0.009). **b.** Box plots showing the values of the slopes of the lines of Fig. 6a for the various samples. An overlap of the raincloud plots is shown on the left-hand side of the plot. The Shapiro-Wilk test showed that all datasets in b) are not normally distributed (all p values < 0.001), and Levene's test showed that variances were equal. The non-parametric Kruskal-Wallis test indicates that data in b) are not statistically different. **c.** Key steps of a coalescence event during flow recorded in the sample with 0.12 wt% of ZnO. The droplets move along the x direction while lying on planes at different z. Droplet 1 moves faster and collides with droplet 2 (c_1). Scale bar is equal to 10 μm. The collision causes a rearrangement of the ZnO nanoparticles, which drift on the droplet surfaces leaving a nanoparticle-free circular-shaped region at the center of droplet 2 (c_2). When the matrix film separating the droplets in this region has become thin enough, it pierces and the two droplets begin merging through the neck, whose section appears as a bright circle (c_3). The neck grows while dragging the nanoparticles (c_4). At the end of process, the nanoparticles lie on the surface of the final droplet (c_5). The full video is available as Supplementary material, V3. (For interpretation of the references to colour in this figure legend, the reader is referred to the web version of this article.)

the slowest one, i.e. at $\theta_m > 90^\circ$. This means that the coalescence process was completed while the hydrodynamic forces pushed the droplets apart, in apparent violation of the film drainage mechanism [53]. Analytical models and simulations predict that the matrix film that separates the colliding droplets is not flat [58–60], and the local thinning could be so pronounced to lead to the reaching of the critical film thickness h_c even when the droplets are moving away [15]. Experimental observations of such a phenomenon, however, are rare and have been mostly related to the presence of surfactants, which could make the film particularly dimpled/deformed [61–63]. Differently, in the present study, coalescence for $\theta_m > 90^\circ$ are due to the bridging ability of the nanoparticles, which keep colliding droplets in contact long enough to allow drainage of the matrix film even when the collision starts at unfavorable angles (i.e. at high θ_c, see Fig. 5b) at which bare droplets would collide without coalescing. To quantify the importance of the bridge-to-drain mechanism, the values of the contact angles at coalescence are shown in Fig. 7 as a function of the nanoparticle content. Three frames of a video showing a representative coalescence event occurred at $\theta_m > 90^\circ$ are also shown.

3.4. Evolution of droplet coverage factor and saturation effect

The possibility of coalescing in a wider range of θ_m (even at $\theta_m > 90^\circ$), results in a substantial increase of the coalescence efficiency. The ability of the nanoparticles to promote coalescence, however, apparently decreases in the sample with 0.21 wt% of nanoparticles (Fig. 4c). It should be noted that saturation effect is not solely related to the initial content of nanoparticles. Each coalescence event, in fact, generates a final droplet whose surface is smaller than the sum of the surfaces of the initial droplets. The surface reduction depends on the ratio between the radii of the initial droplets, reaching a maximum of 20 % when equally sized droplets coalesce (see Supplementary material, S8). A direct consequence of such interface reduction is that, as coalescence proceeds, the nanoparticles must accommodate a smaller and smaller droplet-matrix interface, possibly crowding. We define a droplet coverage factor, Σ_c, as the percentage of droplet surface covered by the ZnO nanoparticles. Quantifying Σ_c and monitoring it during coarsening is difficult. Even assuming that the particles form a monolayer on the droplet surface, for the case at hand of polydisperse, irregularly shaped nanoparticles, Σ_c depends on the packing factor of the surface aggregates (see Fig. 2). Further uncertainty stems from possible effects of the interface curvature, which could differentiate the degree of coverage of small and big droplets. Despite all this complexity, a reasonable expression for Σ_c can be derived resorting to scaling arguments. Assuming monodispersity for both droplets and nanoparticles, each sample can be depicted as a suspension of N droplets (mass M and radius R) partially covered by n nanoparticles (mass m and equivalent radius r; the latter is defined as the radius of the circle having the same area as the projection of the non-circular nanoparticle on the surface of the droplet). The overall surface of all droplets is proportional to N times the surface of the single droplet ($\sim R^2$), while the surface covered by the nanoparticles is proportional to n times the projection of the single nanoparticle on the droplet surface (r^2). Note that the latter proportionality holds irrespective of the shape of the nanoparticles and the way they are assembled onto the droplet surface. Therefore, at any instant the average drop coverage factor can be expressed as:

$$\Sigma_c \propto \frac{nr^2}{NR^2} \tag{5}$$

Since the total mass of droplets ($M_{tot} = N \times M$) and nanoparticles ($m_{tot} = n \times m$) does not change as coalescence proceeds, we can express n and N in terms of m_t and M_t, respectively. Keeping in mind that $M \propto R^3$ and $m \propto r^3$, Eq. (5) can be rewritten as:

$$\Sigma_c \propto \frac{m_{tot}/m}{M_{tot}/M}\frac{r^2}{R^2} \propto \phi R^* \tag{6}$$

in which $\phi = \frac{m_{tot}}{M_{tot}}$ is the mass fraction on nanoparticles with respect to the droplet phase, and $R^* = \frac{R}{r}$ is radius of the droplet made dimensionless by dividing it by the equivalent radius of the nanoparticle. A different approach led to a similar linear relationship even for concentrated emulsions stabilized by monodisperse silica particles [64]. Going back to Eq. (6), since R^* increases during coalescence, so does Σ_c, eventually approaching a threshold, $\Sigma_{c-cr} \sim \phi R^*_\infty$, at which further coalescence is inhibited because of interfacial saturation. This picture is corroborated by the fact that Σ_{c-cr} is the same for the samples containing 0.12 and 0.21 wt% of ZnO: setting $r = 50$ nm as the equivalent nanoparticle radius and $R_\infty = 25$ μm and 15 μm the limiting droplet radii for the samples at $\phi = 0.03$ and 0.05, respectively (see Fig. 4c), a common value of $\Sigma_{c-cr} \approx 7.5$ is obtained. This suggests that the arrest of coalescence in these two samples is the result of interfacial saturation. Differently, the sample at 0.04 wt% of ZnO stops coarsening at $\Sigma_{c-cr} \approx 1.8$ (setting $R_\infty \approx 20$ μm). This means that this sample contains a too low amount of nanoparticles to reach interfacial saturation, and coalescence slows down and eventually arrest for the same mechanisms as in unfilled blends, i.e. because of the combination of increased in the drainage time ($\tau_d \sim R^{13/6}$, see Eq. (4)) and decrease in the collision frequency ($C \sim R^{-3}$). Nonetheless, the comparison with the unfilled blend in Fig. 4c demonstrates that even negligible amounts of nanoparticles exhibit a huge capacity to speed up coalescence. The key factors seem to be (*i*) the partial interfacial coverage and (*ii*) the bridging capacity of the selected ZnO nanoparticles. The principle, however, is general and could apply to other systems with very small amounts of (nano)particles with higher affinity for the matrix phase accumulated at the droplet-matrix

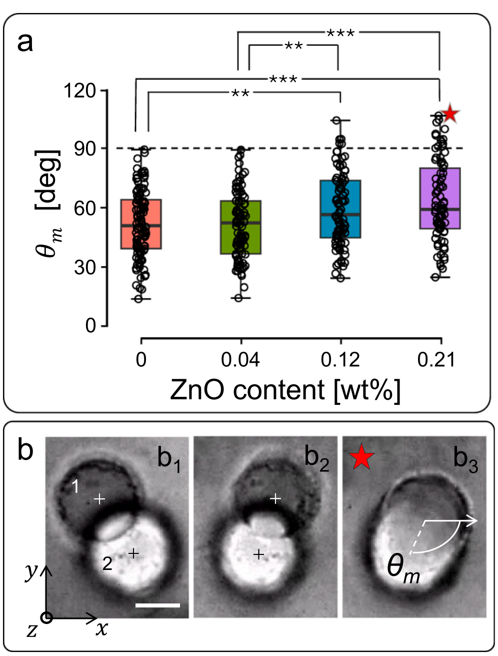

Fig. 7. a. Collision angles at coalescence as a function of the nanoparticle content. Sample size: $n = 106$ (without ZnO nanoparticles), 92 (0.04 wt% of ZnO), 85 (0.12 wt%), and 81 (0.21 wt%). Coalescence occurring at $\theta_m > 90^\circ$ was recorded in the samples at ZnO content of 0.12 and 0.21 wt%. Welch's t-tests indicated statistically relevant differences ($^{**}p < 0.01$ or $^{***}p < 0.001$) between the average θ_m values of the samples without or at low ZnO content (0.04 wt%) and of those at high ZnO content (0.12 and 0.21 wt%). **b.** Frames taken from a representative video of a coalescence event occurred at $\theta_m \cong 107^\circ$ in the sample at 0.21 wt% (red star in Fig. 7a). Droplet 1 moves along the x axis faster than droplet 2. Frame b_3 shows the instant at which the two droplets coalesce. Scale bar is equal to 10 μm. (For interpretation of the references to colour in this figure legend, the reader is referred to the web version of this article.)

interface. Since the destabilizing ability vanishes when the surface coverage factor exceeds Σ_{c-cr}, the same (nano)particles can behave like coalescence promoter or inhibitor depending on their content and of the size of the droplets, representing a versatile tool for a clever manipulation of the morphology of emulsions and blends.

4. Conclusions

The stabilizing effect of nanoparticles at the liquid–liquid interface of emulsions and blends is well known [1–8]. This work has elucidated the microscopic mechanisms underlying the opposite effect, namely the ability of nanoparticles to promote coalescence in the scarcely explored regime of very low loadings [28,30,31]. To this end, tiny amounts of ZnO nanoparticles (up to ~0.2 wt%) were driven onto the surface of micrometric PDMS droplets suspended in a PB matrix (PDMS/PB 4/96 v/v) by a two-step mixing protocol, and the resulting blends were subjected to slow flow ($\dot{\gamma} = 1\ s^{-1}$) to induce coalescence. Despite the higher affinity of the nanoparticles for the matrix phase (which normally leads to a strong stabilization effect [22,23,32]) and their negligible effect on rheology and interfacial energy, only 0.12 wt% of nanoparticles led to a doubling of the coalescence rate and extent. The physics underlying this phenomenon was elucidated thanks to the on-line observation of hundreds of coalescence events using a microfluidic device. In this way, we were able to rule out some of the hypotheses made in the past based on ex-post analyses of droplet morphology (e.g. bridging-dewetting [30,31] or changes in van der Waals attraction between droplets due to particle adsorption [34]), and defined a novel "bridge-to-drain" mechanism based on the bridging ability of nanoparticles, which is necessary to keep colliding droplets in contact long enough to drain the matrix film. Accordingly, even collisions at unfavorable angles, where the bare droplets would stay in contact for too short time, become effective and lead to coalescence. Furthermore, coalescence was also observed when the fastest droplet overtook the slowest, meaning that the matrix film is pulled away instead of being squeezed. However, bridging alone is not sufficient to promote coalescence. Indeed, we have shown that the presence of sufficiently large nanoparticle-free regions is a second necessary condition for droplet merging. This explains why the phenomenon can only be observed with very small amounts of nanoparticles, which tend to act as stabilizers at higher loadings. More importantly, since the liquid–liquid interface decreases as coalescence progresses, a critical droplet coverage fraction was defined at which the nanoparticles stop promoting coalescence and start acting as stabilizers, establishing an equilibrium droplet size. Such a dual capability could be used to fine-tune the droplet size of emulsions and blends. In this context, further targeted studies are needed to clarify the role of parameters related to the nanoparticles, such as size, shape, surface chemistry, charge and roughness, as well as to evaluate the effects of flow conditions, e.g. shear rate and elongational components.

CRediT authorship contribution statement

Angela Marotta: Writing – original draft, Visualization, Validation, Investigation, Data curation. **Valentina Preziosi:** Writing – review & editing, Writing – original draft, Visualization, Validation, Investigation, Data curation. **Giovanna Tomaiuolo:** Writing – review & editing, Visualization, Supervision, Methodology, Data curation, Conceptualization. **Giovanni Filippone:** Writing – review & editing, Writing – original draft, Supervision, Project administration, Methodology, Funding acquisition, Formal analysis, Conceptualization.

Declaration of competing interest

The authors declare that they have no known competing financial interests or personal relationships that could have appeared to influence the work reported in this paper.

Acknowledgements

This study was supported by the Italian Ministry of University and Research (MIUR) through the funding of the project CLEAN – Valorizing Sustainable Plastics through a CLEver use of nANoparticles, prot. 20174FSRZS_003.

Appendix A. Supplementary data

Supplementary data to this article can be found online at https://doi.org/10.1016/j.jcis.2025.02.122.

Data availability

Data will be made available on request.

References

[1] D.J. McClements, Food Emulsions: Principles, Practices, and Techniques, CRC press, 2004. Doi: 10.1201/9781420039436.
[2] S. Tcholakova, Z. Valkova, D. Cholakova, Z. Vinarov, I. Lesov, N. Denkov, S. K. Smoukov, Efficient self-emulsification via cooling-heating cycles, Nat. Commun. 8 (1) (2017) 15012, https://doi.org/10.1038/ncomms15012.
[3] I.F. Guha, S. Anand, K.K. Varanasi, Creating nanoscale emulsions using condensation, Nat. Commun. 8 (1) (2017) 1371, https://doi.org/10.1038/s41467-017-01420-8.
[4] T. Sheth, S. Seshadri, T. Prileszky, M.E. Helgeson, Multiple nanoemulsions, Nat. Rev. Mater. 5 (3) (2020) 214–228, https://doi.org/10.1038/s41578-019-0161-9.
[5] A.J. Ryan, Designer polymer blends, Nat. Mater. 1 (1) (2002) 8–10, https://doi.org/10.1038/nmat720.
[6] T. Kietzke, D. Neher, K. Landfester, R. Montenegro, R. Güntner, U. Scherf, Novel approaches to polymer blends based on polymer nanoparticles, Nat. Mater. 2 (6) (2003) 408–412, https://doi.org/10.1038/nmat889.
[7] T. Uemura, T. Kaseda, Y. Sasaki, M. Inukai, T. Toriyama, A. Takahara, H. Jinnai, S. Kitagawa, Mixing of immiscible polymers using nanoporous coordination templates, Nat. Commun. 6 (1) (2015) 7473, https://doi.org/10.1038/ncomms8473.
[8] C.L. Tucker Iii, P. Moldenaers, Microstructural evolution in polymer blends, Ann. Rev. Fluid Mech. 34 (1) (2002) 177–210, https://doi.org/10.1146/annurev.fluid.34.082301.144051.
[9] R. Zolfaghari, A. Fakhru'l-Razi, L.C. Abdullah, S.S. Elnashaie, A. Pendashteh, Demulsification techniques of water-in-oil and oil-in-water emulsions in petroleum industry, Separat. Purif. Technol. 170 (2016) 377–407, https://doi.org/10.1016/j.seppur.2016.06.026.
[10] A.M. Sousa, M.J. Pereira, H.A. Matos, Oil-in-water and water-in-oil emulsions formation and demulsification, J. Pet. Sci. Eng. 210 (2022) 110041, https://doi.org/10.1016/j.petrol.2021.110041.
[11] A.K. Chesters, Modelling of coalescence processes in fluid-liquid dispersions: a review of current understanding, Chem. Eng. Res. Des. 69 (A4) (1991) 259–270.
[12] L. Hohl, S. Röhl, D. Stehl, R. von Klitzing, M. Kraume, Influence of nanoparticles and drop size distributions on the rheology of w/o Pickering emulsions, Chem. Ing. Tech. 88 (2016) 1815–1826, https://doi.org/10.1002/cite.201600063.
[13] P. Finkle, H.D. Draper, J.H. Hildebrand, The theory of emulsification1, J. Am. Chem. Soc. 45 (1923) 2780–2788.
[14] R. Aveyard, B.P. Binks, J.H. Clint, Emulsions stabilised solely by colloidal particles, Adv. Colloid Interface Sci. 100 (2003) 503–546, https://doi.org/10.1016/S0001-8686(02)00069-6.
[15] E. Chatzigiannakis, N. Jaensson, J. Vermant, Thin liquid films: Where hydrodynamics, capillarity, surface stresses and intermolecular forces meet, Curr. Opin. Colloid Interface Sci. 53 (2021) 101441, https://doi.org/10.1016/j.cocis.2021.101441.
[16] C. Mao, M. Kong, Q. Yang, G. Li, Y. Huang, Droplet coalescence and clustering behavior in microsphere-filled polymeric emulsions under shear flow: the key role of asymmetric interfacial affinities, PCCP 18 (6) (2016) 4429–4436, https://doi.org/10.1039/C5CP07728A.
[17] A. Maani, P.J. Carreau, Rheological and morphological properties of thermoplastic olefin blends containing nanosilica, J. Nonnewton. Fluid Mech. 233 (2016) 95–106, https://doi.org/10.1016/j.jnnfm.2016.01.017.
[18] G.G. Fuller, J. Vermant, Complex fluid-fluid interfaces: rheology and structure, Annu. Rev. Chem. Biomol. Eng. 3 (2012) 519–543, https://doi.org/10.1146/annurev-chembioeng-061010-114202.
[19] S. Vandebril, J. Vermant, P. Moldenaers, Efficiently suppressing coalescence in polymer blends using nanoparticles: role of interfacial rheology, Soft Matter 6 (14) (2010) 3353–3362, https://doi.org/10.1039/B927299B.
[20] T.N. Hunter, R.J. Pugh, G.V. Franks, G.J. Jameson, The role of particles in stabilising foams and emulsions, Adv. Colloid Interface Sci. 137 (2) (2008) 57–81, https://doi.org/10.1016/j.cis.2007.07.007.
[21] P. Thareja, S. Velankar, Particle-induced bridging in immiscible polymer blends, Rheol. Acta 46 (2007) 405–412, https://doi.org/10.1007/s00397-006-0130-2.

[22] T.S. Horozov, B.P. Binks, Particle-stabilized emulsions: a bilayer or a bridging monolayer? Angew. Chem. 118 (5) (2006) 787–790, https://doi.org/10.1002/ange.200503131.

[23] E.J. Stancik, G.G. Fuller, Connect the drops: Using solids as adhesives for liquids, Langmuir 20 (12) (2004) 4805–4808, https://doi.org/10.1021/la049778e.

[24] E. Vignati, R. Piazza, T.P. Lockhart, Pickering emulsions: interfacial tension, colloidal layer morphology, and trapped-particle motion, Langmuir 19 (17) (2003) 6650–6656, https://doi.org/10.1021/la034264l.

[25] G.C. Frye, J.C. Berg, Antifoam action by solid particles, J. Colloid Interface Sci. 127 (1) (1989) 222–238, https://doi.org/10.1016/0021-9797(89)90023-4.

[26] P.R. Garrett, The Science of Defoaming: Theory, Experiment and Applications, CRC Press, 2016.

[27] R. Pugh, Foaming, foam films, antifoaming and defoaming, Adv. Colloid Interface Sci. 64 (1996) 67–142, https://doi.org/10.1016/0001-8686(95)00280-4.

[28] E. Dickinson, Interfacial particles in food emulsions and foams, Colloidal Particles Liquid Interfaces (2006) 298–327, https://doi.org/10.1017/CBO9780511536670.009.

[29] N.D. Denkov, K.G. Marinova, Antifoam effects of solid particles, oil drops and oil-solid compounds in aqueous foams, Colloidal Particles Liquid Interfaces (2006) 383–444, https://doi.org/10.1017/CBO9780511536670.011.

[30] C. Griffith, H. Daigle, Destabilizing Pickering emulsions using fumed silica particles with different wettabilities, J. Colloid Interface Sci. 547 (2019) 117–126, https://doi.org/10.1016/j.jcis.2019.03.048.

[31] P. Thareja, K. Moritz, S.S. Velankar, Interfacially active particles in droplet/matrix blends of model immiscible homopolymers: Particles can increase or decrease drop size, Rheol. Acta 49 (2010) 285–298, https://doi.org/10.1007/s00397-009-0421-5.

[32] N.P. Ashby, B.P. Binks, V.N. Paunov, Bridging interaction between a water drop stabilised by solid particles and a planar oil/water interface, Chem. Commun. 4 (2004) 436–437, https://doi.org/10.1039/B314004K.

[33] P. Thareja, S. Velankar, Rheology of immiscible blends with particle-induced drop clusters, Rheol. Acta 47 (2008) 189–200, https://doi.org/10.1007/s00397-007-0231-6.

[34] S. Nagarkar, S.S. Velankar, Rheology and morphology of model immiscible polymer blends with monodisperse spherical particles at the interface, J. Rheol. 57 (3) (2013) 901–926, https://doi.org/10.1122/1.4801757.

[35] S.P. Nagarkar, S.S. Velankar, Morphology and rheology of ternary fluid–fluid–solid systems, Soft Matter 8 (32) (2012) 8464–8477, https://doi.org/10.1039/C2SM25758K.

[36] A. Schröder, J. Sprakel, K. Schroën, J.N. Spaen, C.C. Berton-Carabin, Coalescence stability of Pickering emulsions produced with lipid particles: A microfluidic study, J. Food Eng. 234 (2018) 63–72, https://doi.org/10.1016/j.jfoodeng.2018.04.007.

[37] E. Moghimi, F. Goharpey, R. Foudazi, Role of droplet bridging on the stability of particle-containing immiscible polymer blends, Rheol. Acta 53 (2014) 165–180, https://doi.org/10.1007/s00397-013-0752-0.

[38] T.M. Ho, A. Razzaghi, A. Ramachandran, K.S. Mikkonen, Emulsion characterization via microfluidic devices: A review on interfacial tension and stability to coalescence, Adv. Colloid Interface Sci. 299 (2022) 102541, https://doi.org/10.1016/j.cis.2021.102541.

[39] Y. Stern, R. Tadmor, V. Multanen, G. Oren, A first order-based model for the kinetics of formation of Pickering emulsions, J. Colloid Interface Sci. 628 (2022) 409–416, https://doi.org/10.1016/j.jcis.2022.07.11.

[40] C.A. Schneider, W.S. Rasband, K.W. Eliceiri, NIH Image to ImageJ: 25 years of image analysis, Nat. Methods 9 (7) (2012) 671–675, https://doi.org/10.1038/nmeth.2089.

[41] H.P. Grace, Dispersion phenomena in high viscosity immiscible fluid systems and application of static mixers as dispersion devices in such systems, Chem. Eng. Commun. 14 (3–6) (1982) 225–277, https://doi.org/10.1080/00986448208911047.

[42] R. D'Apolito, A. Perazzo, V. Preziosi, M. D'Antuono, G. Tomaiuolo, R. Miller, S. Guido, Measuring interfacial tension of emulsions in situ by microfluidics, Langmuir 34 (2018) 4991–4997, https://doi.org/10.1021/acs.langmuir.8b00208.

[43] A. Taguet, P. Cassagnau, J.-M. Lopez-Cuesta, Structuration, selective dispersion and compatibilizing effect of (nano) fillers in polymer blends, Prog. Polym. Sci. 39 (8) (2014) 1526–1563, https://doi.org/10.1016/j.progpolymsci.2014.04.002.

[44] J. Plattier, L. Benyahia, M. Dorget, F. Niepceron, J.-F. Tassin, Viscosity-induced filler localisation in immiscible polymer blends, Polymer 59 (2015) 260–269, https://doi.org/10.1016/j.polymer.2014.12.044.

[45] B.P. Binks, Particles as surfactants — similarities and differences, Curr. Opin. Colloid Interface Sci. 7 (1–2) (2002) 21–41, https://doi.org/10.1016/S1359-0294(02)00008-0.

[46] E.J. Stancik, M. Kouhkan, G.G. Fuller, Coalescence of particle-laden fluid interfaces, Langmuir 20 (1) (2004) 90–94, https://doi.org/10.1021/la0356093.

[47] H. Xu, M. Lask, J. Kirkwood, G. Fuller, Particle bridging between oil and water interfaces, Langmuir 23 (9) (2007) 4837–4841, https://doi.org/10.1021/la063593l.

[48] L. Botto, E.P. Lewandowski, M. Cavallaro, K.J. Stebe, Capillary interactions between anisotropic particles, Soft Matter 8 (39) (2012) 9957–9971, https://doi.org/10.1039/C2SM25929J.

[49] H. Lehle, M. Oettel, Stability and interactions of nanocolloids at fluid interfaces: effects of capillary waves and line tensions, J. Phys. Condens. Matter 20 (40) (2008) 404224, https://doi.org/10.1088/0953-8984/20/40/404224.

[50] Y. Liao, D. Lucas, A literature review on mechanisms and models for the coalescence process of fluid particles, Chem. Eng. Sci. 65 (10) (2010) 2851–2864, https://doi.org/10.1016/j.ces.2010.02.020.

[51] M.V. Smoluchowski, Versuch einer mathematischen Theorie der Koagulationskinetik kolloider Lösungen, Zeitschrift Für Physikalische Chem. 92 (1) (1918) 129–168, https://doi.org/10.1515/zpch-1918-9209.

[52] R. Shinnar, J.M. Church, Statistical theories of turbulence in predicting particle size in agitated dispersions, Ind. Eng. Chem. 52 (3) (1960) 253–256, https://doi.org/10.1021/ie50603a036.

[53] P.T. Jaeger, J. Janssen, F. Groeneweg, W. Agterof, Coalescence in emulsions containing inviscid drops with high interfacial mobility, Colloids Surf. A Physicochem. Eng. Asp. 85 (2–3) (1994) 255–264, https://doi.org/10.1016/0927-7757(94)02848-6.

[54] P.C. Van der Hoeven, J. Lyklema, Electrostatic stabilization in non-aqueous media, Adv. Colloid Interface Sci. 42 (1992) 205–277, https://doi.org/10.1016/0001-8686(92)80024-R.

[55] W.H. Briscoe, R.G. Horn, Direct measurement of surface forces due to charging of solids immersed in a nonpolar liquid, Langmuir 18 (10) (2002) 3945–3956, https://doi.org/10.1021/la015657s.

[56] D.E. Tambe, M.M. Sharma, The effect of colloidal particles on fluid-fluid interfacial properties and emulsion stability, Adv. Colloid Interface Sci. 52 (1994) 1–63, https://doi.org/10.1016/0001-8686(94)80039-1.

[57] A.B. Pawar, M. Caggioni, R. Ergun, R.W. Hartel, P.T. Spicer, Arrested coalescence in Pickering emulsions, Soft Matter 7 (17) (2011) 7710–7716, https://doi.org/10.1039/C1SM05457K.

[58] Y. Yoon, F. Baldessari, H.D. Ceniceros, L.G. Leal, Coalescence of two equal-sized deformable drops in an axisymmetric flow, Phys. Fluids 19 (10) (2007), https://doi.org/10.1063/1.2772900.

[59] A. Lai, N. Bremond, H.A. Stone, Separation-driven coalescence of droplets: an analytical criterion for the approach to contact, J. Fluid Mech. 632 (2009) 97–107, https://doi.org/10.1017/S0022112009007320.

[60] D.Y. Chan, E. Klaseboer, R. Manica, Dynamic interactions between deformable drops in the Hele–Shaw geometry, Soft Matter 6 (8) (2010) 1809–1815, https://doi.org/10.1039/B918933E.

[61] B. Dai, L.G. Leal, The mechanism of surfactant effects on drop coalescence, Phys. Fluids (1994-present) 20(4) (2008) 040802. doi: 10.1063/1.2911700.

[62] L.G. Leal, Droplet coalescence and breakup with application to polymer blending, J. Cent. South Univ. Technol. 14 (Suppl 1) (2007) 1–5, https://doi.org/10.1007/s11771-007-0201-2.

[63] L.G. Leal, Flow induced coalescence of drops in a viscous fluid, Phys. Fluids (1994-present) 16 (6) (2004) 1833–1851, https://doi.org/10.1063/1.1701892.

[64] S. Arditty, C. Whitby, B. Binks, V. Schmitt, F. Leal-Calderon, Some general features of limited coalescence in solid-stabilized emulsions, European Phys. J. E 11 (2003) 273–281, https://doi.org/10.1140/epje/i2003-10018-6.